Journal of Signal Processing Systems (2026) 98:2
https://doi.org/10.1007/s11265-025-01971-w

# Tracking Scheme for Monitoring Indoor Scene using Distributed mmWave MIMO Radar Sensors

**Uday Kumar Singh[1] · Moein Ahmadi[2] · Rangeet Mitra[3] · K Venkateswaran[3] · Rama Rao Thipparaju[4]**

Received: 22 January 2025 / Revised: 10 September 2025 / Accepted: 16 October 2025


**Abstract**
While millimeter wave (mmWave) multiple input multiple output (MIMO) radars are increasingly popular for their compact size and resilience to varying lighting conditions, their limited field of view (FOV) restricts their coverage. This limitation can be overcome by employing a multisensor network that utilizes multiple mmWave MIMO radars to expand surveillance coverage. Although several detection methods have been proposed for distributed mmWave radar networks, a unified tracking solution for continuous-time monitoring has not been fully explored. To address this gap, this paper introduces a novel tracking framework for mmWave MIMO radar networks, specifically designed to overcome the limitations of single-sensor systems in indoor environments. The paper presents a customized multi-target tracking (MTT) scheme that tackles artifacts in the detection scheme such as false alarms and missed detections that are caused by limited FOV of individual sensors. The proposed MTT scheme processes data from a newly developed detector that integrates measurements from multiple radars. The computational complexity of the proposed MTT scheme is derived. The effectiveness of the proposed tracking approach is validated through extensive computer simulations, focusing on metrics such as root mean square error and the number of maintained target tracks. The performance of the proposed approach has exceeded the classical approach with a significant improvement in the context of targets' detection and tracking. Furthermore, with the study presented, the article concludes that the optimal performance of the MTT is obtained if the detector produces detections with a probability of false alarm $P_{fa} \leq 10^{-5}$.

**Keywords** Clutter · FOV · MIMO Radar · MTT · mmWave

## 1 Introduction

In recent days, millimeter wave (mmWave) multiple input multiple output (MIMO) radar has proven its worth for various civilian and industrial applications, ranging from monitoring human presence in indoor environments to making vehicles and machines autonomous. This wide range of applications is possible because of the wider bandwidth of the mmWave MIMO radar, which provides a finer resolution. Also, the higher center frequency, typically in

Moein Ahmadi, Rangeet Mitra, K Venkateswaran, and Rama Rao Thipparaju contributed equally to this work.

✉ Uday Kumar Singh
udaykumar.singh@sru.edu.in

Moein Ahmadi
moein.ahmadi@uni.lu

Rangeet Mitra
rangeet.m@cmrit.ac.in

K Venkateswaran
venkateswaran.k@cmrit.ac.in

Rama Rao Thipparaju
ramaraot@srmist.edu.in

[1] Department of ECE, SR University, Warangal, Telengana 506371, India

[2] SnT, University of Luxembourg, JFK, Luxembourg 1359, Luxembourg

[3] Department of ECE, CMR Institute of Technology, Bengaluru 560037, Karnataka, India

[4] Department of ECE, SRM University, 522502 Amravati, India

Published online: 19 November 2025

the GHz range, allows a broader Doppler spectrum coverage and refines the micro-Doppler resolution. Specifically, for indoor monitoring, the mmWave MIMO radar is particularly effective, as it can detect the movement of targets moving at very slow speeds. However, a single radar has a limited field of view (FOV) due to its small antenna size or limited transmitted power, restricting its ability to fully cover the surveillance area. A viable solution is to use a network of distributed though connected mmWave radar sensors. This distributed radar configuration not only enhances coverage of the surveillance area, but also exploits geometric and spatial diversity to improve target detection performance. The improved target detection would enhance the performance of subsequent signal processing steps, such as tracking.

In a radar system, the received signal typically comprises various elements, including targets' data, clutter echoes, receiver noise, and neighboring radar interference. In both network-based radar systems and single-sensor systems, the detection task involves analyzing the echo data to determine the presence of a target. The [1–7] are some of the relevant literature that focuses on target detection. In particular, in [8], the authors considered a clutter environment and explored the detection of moving targets amid clutter. The cluttered environment is assumed to be spatially nonhomogeneous, also, each radar was considered to be monostatic (transmitter and receiver are colocated) and the interference signal is modeled in the Doppler frequency domain. In the same line of research, [9] investigates the detection of moving targets using a phased MIMO radar mounted on an airborne platform.

Building on previous research, a low complexity detector for indoor scenarios using a single monostatic radar was introduced in [10]. In addition, [11] explores a 3D constant false alarm rate (CFAR) algorithm designed to detect drones with a co-located MIMO radar, without employing a network-based radar system. Furthermore, [12] presents a two-level CFAR detector for the mmWave radar that does not account for interference subspace. Similarly, [13] develops a CFAR detector for a single radar with a general antenna array configuration, incorporating primary and reference channels with high and low gain beams, respectively. In contrast to these previous works, [14] introduces an optimal detector for a group of MIMO radar sensors aimed at monitoring indoor environments. This detector is designed to identify moving targets amid interference, clutter, and noise, as shown in Figure 1. The detector proposed in [14] demonstrates superior performance compared to existing detectors not based on subspace.

With the aforementioned short survey, it is evident that the development of tracking schemes post-detection and analyzing their performance for the network of mmWave MIMO radar remains an open challenge. The existing literature [15–18] talks only about the scheme of assigning detections to tracks and is limited to improve only the data association techniques. In practice, apart from assigning detections to the tracks, the tracker is responsible for the track maintenance, which includes successful generation and deletions of tracks. However, the existing literature lacks complete information on the steps involved in the evolution of detections to tracks. To address this gap, we have designed a multiple target tracker (MTT) to complete the signal processing chain for the mmWave MIMO radar network and demonstrate its efficacy using the detection scheme proposed in [14]. The designed tracker serves as a post-processing step, linking consecutive detector detections to provide continuous monitoring and producing meaningful tracks and kinematic information of the detected targets in 2 D [19], along with removing unnecessary tracks whenever required. The computational complexity of the proposed tracking scheme is also derived in the presented article.

To address the scenario of monitoring an indoor scene using a network of mmWave radar sensors, a signal model is developed that integrates signal-dependent and signal-independent interferences. These interferences are characterized by variable coefficients determined by factors such as geometry and reflectivity. Based on this model, the generalized likelihood ratio test (GLRT) detector from [14] is reviewed, including its statistical attributes. Following this, an MTT scheme is introduced, which leverages the detections obtained using the method described in [14]. Recognizing that clutter and interference can lead to false alarms and negatively affect radar performance, the proposed tracking system is designed to mitigate these challenges. The core of the MTT system lies in the association of data, which serves as a filter to distinguish sequential target detections from spurious ones. In this study, the nearest-neighbor (NN) algorithm is used, which uses the Mahalanobis distance, for data association. It is important to note that this work focuses on providing a tracking framework rather than proposing novel data association techniques, which is why the basic NN algorithm is utilized. However, in denser environments where target crossings are more frequent, advanced methods such as Multiple Hypothesis Tracking (MHT) or Joint Probabilistic Data Association (JPDA) may be more appropriate [20]. Once data association is performed, the matched detections are used to update tracks via the Kalman Filter (KF) or its nonlinear extensions, such as the Unscented Kalman Filter (UKF), Particle Filter, or Extended Kalman Filter (EKF), depending on whether the observations are in Cartesian

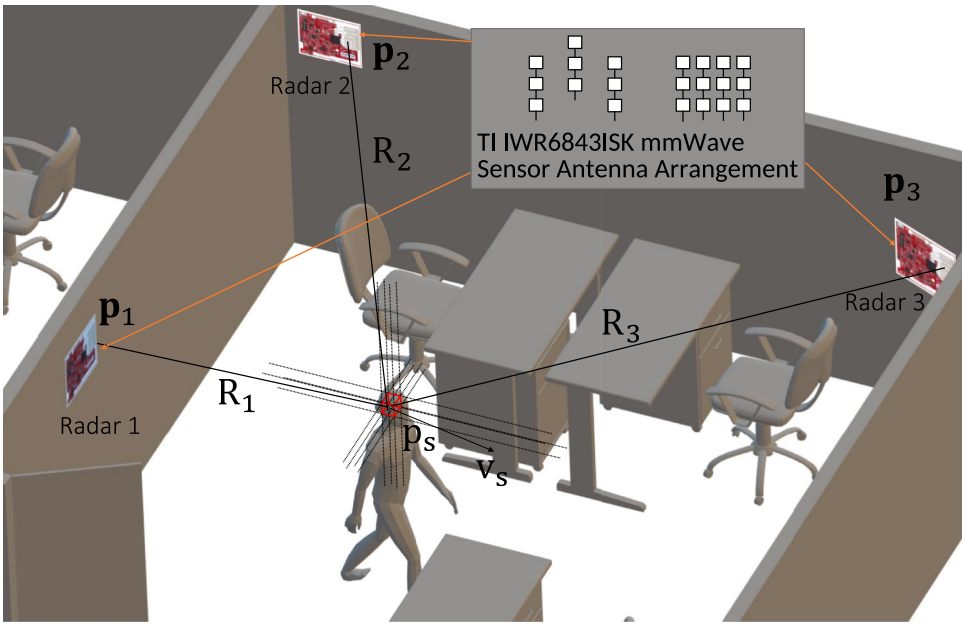


**Fig. 1** Monitoring Indoor Environment Using Multiple Distributed MIMO Radar Sensors.

or Spherical coordinates [21, 22]. At each radar frame or scan, the DBSCAN clustering algorithm [23] evaluates unassociated detections to determine if they can form new tracks. When DBSCAN identifies sufficient detections, new tracks are initialized. These tracks remain tentative for a predefined duration and are promoted to confirmed tracks if consistently updated during this period; otherwise, they are removed. It is worth mentioning that, contrary to the NN algorithm and DBSCAN, track confirmation and deletion are based on logical rules. Additionally, to model the random movement of targets in indoor environments, the Discrete White Noise Acceleration (DWNA) motion model is used in the KF state estimation equation. The DWNA model helps in modeling the stochastic nature of target motion by incorporating the acceleration variances along different coordinate axes.

The following summarizes the contribution of the proposed work.

1. An MTT tracker is designed to monitor the movement of targets in an indoor environment while managing detection artifacts.
2. The tracker utilizes the detections provided by the detector proposed in [14], thus demonstrating the feasibility of the proposed tracking approach.
3. The developed tracker is capable of generating new tracks and removing invalid ones, effectively managing the dynamic nature of the surveillance scene.
4. The presented study will help determine the appropriate value of the detector probability of false alarm $(P_{fa})$, required to effectively maintain the tracks for the actual number of targets.

The paper is organized as follows. Section 2 outlines the signal model followed by the detection framework based on binary hypothesis testing. It also provides a review of the detector introduced in [14]. Section 3, demonstrates the proposed tracking scheme for multiple targets. The simulation results are demonstrated in Section 4. Lastly, in Section 5, the conclusion of the paper is provided covering the summary of the findings derived from the simulations. The Section 5, also covers the future direction of the presented work.

**Notations** Vectors and matrices are represented by lowercase and uppercase bold letters, respectively. The notation $(.)^T$ and $(.)^H$ are used to denote transpose and Hermitian transpose operations. The identity matrix is represented by I, and the Kronecker product is denoted as $\otimes$. Additionally, the Euclidean norm of a vector is represented as $|.|$. The difference between sets and the empty set is indicated by $\setminus$ and $\emptyset$, respectively. To refer to the $i^{th}$ column of a matrix A, the notation $\mathrm{A}^i$ is used, while $\mathrm{a}^i$ represents the $i^{th}$ element of a vector a. The function $len(\cdot)$ is used to access the number of elements in a vector or the number of columns in a matrix.

Lastly, $\mathbb{R}$ and $\mathbb{N}$ denote the set of real and natural numbers, respectively.

## 2 Signal Model, Problem Formulation, and Detection Test

This section provides an explanation of signal modeling for the data collected from the multiple sensors shown in Figure 1. It also introduces the hypothesis testing problem associated with the signal model. The section concludes with a review of the detection test detailed in [14].

Consider a distributed radar system composed of $L$ co-located mmWave MIMO radar sensors. Each sensor has $N_l$ receiving antenna elements and $M_l$ transmitting antenna elements. The position of the $l^{th}$ radar sensor in the 3D space is indicated by $\mathrm{p}_l = [x_l, y_l, z_l]^T$, where the orthogonal axes $x_l$, $y_l$, and $z_l$ define the coordinate system. An arbitrary target located at $\mathrm{p}_t = [x_t, y_t, z_t]^T$ and moving with a velocity $\mathrm{v}_t = [vx_t, vy_t, vz_t]^T$ as shown in Figure 1 is at a distance $R_l$ from the $l^{th}$ radar sensor. The relative position of the target is also described by its azimuth angle $\theta_l^a$ and elevation angle $\theta_l^e$. In this setup, the response of the $l^{th}$ radar sensor to $Q_l$ transmitted chirps (or pulses) in a single coherent processing interval (CPI) is as follows:

$$\mathrm{r}_l = \alpha_l \mathrm{s}_l(\theta_l^a, \theta_l^e, f_{d,l}) + \mathrm{c}_l + \mathrm{n}_l \in \mathbb{C}^{Q_l N_l M_l} \tag{1}$$

In Eq. 1

$$\alpha_l = \left(\beta_l \frac{P_t G_t G_r \lambda^2 \sigma_l}{(4\pi)^3 R_l^4 L_{sl}}\right)^{\frac{1}{2}} \tag{2}$$

represents the amplitude of the reflected signal at the $l$th radar sensor. In this expression, $\lambda$ is the wavelength, $P_t$ is the transmitted power, and $G_t$ and $G_r$ are the gain in the transmission and reception antennas, respectively. Furthermore, $\sigma_l$ is the radar cross section (RCS) of the $l^{th}$ radar sensor, which varies due to the different viewing angles between the sensors and the target. The term $L_{sl}$ accounts for the combined loss of system and propagation, and $\beta_l$ denotes the impedance of the radar input to the $l^{th}$ receiver.

In Eq. 1, the signal steering vector is represented by $\mathrm{s}_l(\theta_l^a, \theta_l^e, f_{d,l})$, while $\mathrm{c}_l$ and $\mathrm{n}_l$ represent the clutter and noise components, respectively. The noise, denoted as $\mathrm{n}_l \sim \mathcal{CN}(0, \sigma^2 \mathrm{I}) \in \mathbb{C}^{Q_l N_l M_l}$, is assumed to be the ever-present thermal white noise. Consequently, the noise power $\sigma^2$ for a single noise component in $\mathrm{n}_l$ is defined as

$$\sigma^2 = \beta k_B T_0 B F_n \tag{3}$$

where, $k_B$ is the Boltzmann constant, $T_0$ is the effective receiver noise temperature, $B$ is the receiver filter bandwidth, $F_n$ is the receiver noise factor, and the assumption is made that $\beta_l = \beta$.

The signal steering vector for $l^{th}$ radar sensor is given by,

$$\mathrm{s}_l(\theta_l^a, \theta_l^e, f_{d,l}) = \mathrm{a}_l(\theta_l^a, \theta_l^e) \otimes \mathrm{d}_l(\theta_l^a, \theta_l^e) \otimes \mathrm{b}_l(f_{d,l}), \tag{4}$$

where

$$\mathrm{a}_l(\theta^a, \theta^e) = [e^{-j\mathrm{k}^T(\theta^a,\theta^e)\mathrm{p}_{l,1}^{tx}}, \ldots, e^{-j\mathrm{k}^T(\theta^a,\theta^e)\mathrm{p}_{l,M_l}^{tx}}]^T, \tag{5}$$

and

$$\mathrm{b}_l(\theta^a, \theta^e) = [e^{-j\mathrm{k}^T(\theta^a,\theta^e)\mathrm{p}_{l,1}^{rx}}, \ldots, e^{-j\mathrm{k}^T(\theta^a,\theta^e)\mathrm{p}_{l,N_l}^{rx}}]^T, \tag{6}$$

are the transmit and receive spatial steering vectors, respectively, and

$$\mathrm{k}(\theta^a, \theta^e) = \frac{2\pi}{\lambda}[\cos\theta^a \cos\theta^e, \sin\theta^a \cos\theta^e, \sin\theta^e]^T, \tag{7}$$

is the wavenumber vector, the terms $\mathrm{p}_{l,m}^{tx}$ and $\mathrm{p}_{l,n}^{rx}$ denote the positions of the $m^{th}$ transmit element and the $n^{th}$ receive element of the $l^{th}$ radar sensor. Also,

$$\mathrm{d}_l(f_{d,l}) == [1, e^{j2\pi f_{d,l} T_l}, \ldots, e^{j2\pi f_{d,l}(L_q-1)T_l}]^T \tag{8}$$

where $T_l$ is the pulse repetition interval (PRI) and $f_{d,l}$ is the Doppler frequency of the target experienced by the $l^{th}$ radar sensor and can be expressed as, $f_{d,l} = \frac{2\mathrm{v}_t{}^T(\mathrm{p}_l - \mathrm{p}_t)}{\lambda \|\mathrm{p}_l - \mathrm{p}_t\|}$.

For fusion, the signal received by all $L$ radar sensors can be stacked as $\mathrm{r} = [\mathrm{r}_1^T, \mathrm{r}_2^T, ..., \mathrm{r}_L^T]^T$, correspondingly, the signal steering matrix $\mathrm{S} \in \mathbb{C}^{\sum_{l=1}^{L} M_l N_l Q_l \times L}$ is given by[1]

$$\mathrm{S} = \begin{bmatrix} \mathrm{s}_1(\theta_1^a, \theta_1^e, f_{d,1}) & 0_{Q_1 M_1 N_1 \times 1} & \cdots & 0_{Q_1 M_1 N_1 \times 1} \\ 0_{Q_2 M_2 N_2 \times 1} & \mathrm{s}_2(\theta_2^a, \theta_2^e, f_{d,2}) & \cdots & 0_{Q_2 M_2 N_2 \times 1} \\ \vdots & \vdots & \ddots & \vdots \\ 0_{Q_L M_L N_L \times 1} & 0_{Q_L M_L N_L \times 1} & \cdots & \mathrm{s}_L(\theta_L^a, \theta_L^e, f_{d,L}) \end{bmatrix} \tag{9}$$

Thus, the fused received signal can be expressed by,

$$\mathrm{r} = \boldsymbol{\alpha}\mathrm{S}^H + \mathrm{c} + \mathrm{n}, \tag{10}$$

where $\mathrm{c} = [\mathrm{c}_1^T, \mathrm{c}_2^T, ..., \mathrm{c}_L^T]^T$, $\mathrm{n} = [\mathrm{n}_1^T, \mathrm{n}_2^T, ..., \mathrm{n}_L^T]^T$, and $\boldsymbol{\alpha} = [\alpha_1, \alpha_2, ..., \alpha_L]^T$.

Let $\mathrm{c}_l = \mathrm{E}_l \mathrm{g}_l$, where $\mathrm{E}_l \in \mathbb{C}^{M_l N_l Q_l \times H_l}$ defines the interference subspace with $H_l$ as the interference matrix rank. In this case, interference signals depend on the spread of the Doppler spectrum and also on spatial locations of high-RCS stationary scatterers. Assume that the region of

[1] In this work, the fusion is performed at the measurement level.

interference scatterers is $\theta_{l,1}^{a,int} < \theta_l^a < \theta_{l,2}^{a,int}$ in azimuth, $\theta_{l,1}^{e,int} < \theta_l^e < \theta_{l,2}^{e,int}$ in elevation, and $f_{d,l,1}^{int} < fd, l < f_{d,l,2}^{int}$ in Doppler frequency. Then

$$\mathrm{E}_l = [\mathrm{s}_l(\theta_{l,1}^a, \theta_{l,1}^e, f_{d,l,1}), \ldots, \mathrm{s}_l(\theta_{l,H_l}^a, \theta_{l,H_l}^e, f_{d,l,H_l})].$$

In addition, $\mathrm{g}_l \in \mathbb{C}^{H_l \times 1}$ is an unknown complex vector deterministic coefficient related to each column of the matrix $\mathrm{E}_l$. By defining $\mathrm{g} = [\mathrm{g}_1^T, \mathrm{g}_2^T, ..., \mathrm{g}_L^T]^T$, and

$$E \in C^{\sum_{l=1}^{l} M_l N_l Q_l \times \sum_{l=1}^{L} H_l =}$$
$$\begin{bmatrix} E_1 & 0_{Q_1 M_1 N_1 \times H_2} & \cdots & 0_{Q_1 M_1 N_1 \times H_L} \\ 0_{Q_2 M_2 N_2 \times H_1} & E_2 & \cdots & 0_{Q_2 M_2 N2 \times HL} \\ \vdots & \vdots & \ddots & \vdots \\ 0_{Q_L M_L N_L \times H1} & 0_{Q_L M_L N_L \times H_2} & \cdots & E_L \end{bmatrix}$$

After defining E, the interference signal can be expressed as $\mathrm{c} = \mathrm{Eg}$. Let $\mathcal{H}_0$ and $\mathcal{H}_1$ be the hypothesis that the target is absent and the target is present, respectively. Thus, the following binary hypothesis test represents the detection problem.

$$\begin{cases} \mathcal{H}_1 : & \mathrm{r} = \boldsymbol{\alpha}\mathrm{S}^H + \mathrm{c} + \mathrm{n}. \\ \mathcal{H}_0 : & \mathrm{r} = \mathrm{Eg} + \mathrm{n} \end{cases} \tag{11}$$

For the binary hypothesis test problem mentioned in Eq. 11, the detection test is proposed in [14] and the corresponding test statistics is given by

$$t_{\mathrm{AD}} = \frac{K\Omega}{\sum_{k=1}^{K} \mathrm{r}_k \mathrm{P}_{\mathrm{E}}^{\perp} \mathrm{r}_k} \mathrm{r}^H \mathrm{P}_{\mathrm{E}}^{\perp} \mathrm{S} (\mathrm{S}^H \mathrm{P}_{\mathrm{E}}^{\perp} \mathrm{S})^{-1} \mathrm{S}^H \mathrm{P}_{\mathrm{E}}^{\perp} \mathrm{r} \underset{\mathrm{H}_0}{\overset{\mathrm{H}_1}{\gtrless}} \eta, \tag{12}$$

where, $\mathrm{P}_{\mathrm{E}}^{\perp} = \mathrm{I} - \mathrm{E}(\mathrm{E}^H \mathrm{E})^{-1} \mathrm{E}^H$ is the orthogonal projection over the subspace spanned by E, $K$ is the number of neighboring cells around the cell under detection test, and $\Omega = \sum_{l=1}^{L} Q_l M_l N_l$.

The adaptive detector Eq. 12 has the probability of false alarm given by

$$P_{\mathrm{fa-AD}} = \widetilde{I}_{\frac{\eta\Omega}{\eta\Omega + \mathrm{K}\Omega - r}} (\mathrm{L}, \mathrm{K}\Omega - r), \tag{13}$$

where $\widetilde{I}_k(.,.)$ is the regularized incomplete beta function.

The probability of a false alarm presented in Eq. 13 remains unaffected by the statistical properties of the interference, establishing the detector in Eq. 12 as a CFAR detector. The subsequent sections provide a detailed description of the proposed tracking scheme tailored to the detection test Eq. 12 for specific values of probability of detection $(P_d)$ and $P_{fa}$ provided by the detector.

## 3 Proposed MTT Scheme

This section offers a detailed illustration of how to implement the developed tracking algorithm to track the detections resulting from Eq. 12. In particular, the description of various vital components, such as measurement/data association, track maintenance (creation and deletion of tracks), and the role of KF, is explained in detail. In Figure 2, the main tracking steps are presented in their sequential order of appearance.

In the $k^{th}$ CPI frame, it is assumed that the detector reports new $M$ detections $(\mathrm{O}_k \in \mathbb{R}^{2\times M})$ from the surveillance area. These detections $M$ can consist of both target measurements $N$ and false measurements $n_c$, where $n_c$ depends on the level of clutter, which is quantified by the detector's $P_{fa}$. Hence, $M = N + n_c$. In the presence of clutter and interference, which is the case of consideration, the tracker filters out the target-related measurements from $\mathrm{O}_k$, thus eliminating spurious data. In addition to filtering, the proposed technique also involves assigning the filtered measurements to the appropriate tracks and maintaining these tracks, which includes tasks such as initialization, deletion, and updates.

### 3.1 Association of Measurement and Deletion of Tracks

**Associating Measurement** Data association functions as a filter, isolating target detections from $\mathrm{O}_k$. In this work, the NN algorithm is used for association because of its simplicity and suitability for situations where measurements are

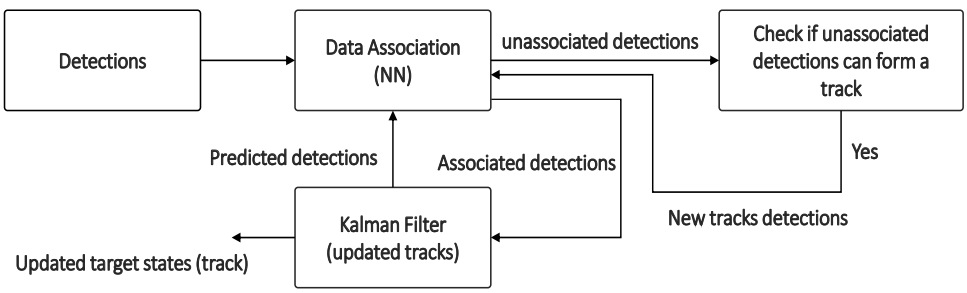


**Fig. 2** Block diagram for the proposed MTT scheme.

sparsely distributed. In the $k^{th}$ time case, given the predicted measurements ($\mathrm{O}_{k-1}^{p} \in \mathbb{R}^{2\times I}$) of the existing tracks $I$ and the new sensor measurements ($\mathrm{O}_k$), the NN algorithm calculates the Mahalanobis distances. The Mahalanobis distance is defined as:

$$\mathcal{M}_{ij} = \exp\left( -(\mathrm{O}_{k-1}^{p^i} - \mathrm{O}_k^j) \sum\nolimits_{k-1}^{i} (\mathrm{O}_{k-1}^{p^i} - \mathrm{O}_k^j)^H \right), \quad \forall i, \forall j \tag{14}$$

where, $\sum_{k-1}^{i}$ is the covariance matrix of $\mathrm{O}_{k-1}^{p^i}$, $i = 1, 2, \ldots, I$ and $j = 1, 2, \ldots, M$ indexing the columns of $\mathrm{O}_{k-1}^{p}$ and $\mathrm{O}_k$, respectively.

For the $i^{th}$ track, the Mahalanobis distances can be arranged as a vector $\mathrm{d}_i = [\mathcal{M}_{i1}, \mathcal{M}_{i2}, \ldots, \mathcal{M}_{ij}, \ldots, \mathcal{M}_{iM}] \in \mathbb{R}^{1\times M}$.. For each track index ($i$), the NN algorithm identifies the measurement with the minimum distance: $j_i^a = \arg\min_j \mathrm{d}_i \ \ \forall i$.. Consequently, a gate test is performed that compares the minimum distance value with a predefined gate radius ($r$). If the distance corresponds to the measurement that validates the test, the index is stored in an associated index array ($\mathrm{i}_a$) as $\mathrm{i}_a = [j_1^a, j_2^a, \ldots, j_j^a, \ldots, j_I^a]$. Consequently, measurements indexed by the elements of $\mathrm{i}_a$, that is, $\mathrm{O}_k^{\mathrm{i}_a}$, are considered associated and processed for updating and filtering. It is important to note that the association of the measurements with their corresponding tracks is a binary decision; in other words, each $i^{th}$ track will be associated with one measurement from $\mathrm{O}_k$ or none at all. This can lead to ambiguity in the NN algorithm when the targets follow cross-trajectories. For such cases, JPDA or MHT would be more appropriate where the association is based on probabilities instead of statistical distance.

After the measurements are associated, in the filtering process, the states of the existing $I$ tracks are updated by the associated measurements using the Kalman filter.

### 3.1.1 Role of the Kalman Filter

In the realm of state estimation, the Kalman filter assumes the evolution of the states for existing $I$ tracks as

$$\mathrm{s}_k^{i_a} = \mathrm{g}(\mathrm{s}_{k-1}^{i_a}) + \mathbf{\Gamma}_a \mathrm{u}_k, \forall i_a \in [1, 2, \cdots, I] \tag{15}$$

where, $\mathrm{s}_{k-1}^{i_a}$ denotes the state vector of the $i_a^{th}$ track in the previous time step and consist of the target's positions in 2D space $(x_k^{i_a}, y_k^{i_a})$ and their corresponding constant velocities $(v_{x_k}^{i_a}, v_{y_k}^{i_a})$, $\mathrm{g}(\cdot) \in \mathbb{R}^{n_s\times 1}$ represents the state evolution, which is modeled using constant velocity (CV). The term $\mathrm{u}_k \in \mathbb{R}^{2\times 1}$ captures random accelerations in both the $x$ and $y$ directions. Furthermore, $\mathrm{u}_k$ is the Gaussian random process sample that has zero mean and a known covariance matrix $\mathrm{U} = \mathbb{E}[\mathrm{u}_k \mathrm{u}_k^T] = \begin{bmatrix} \sigma_{a_x} & 0 \\ 0 & \sigma_{a_y} \end{bmatrix}$, such that $\mathrm{u}_k \sim \mathcal{N} \in \mathbb{R}(0, \mathrm{U})$. Further, in Eq. 15, $\mathrm{g}(\mathrm{s}_{k-1}^{i_a}) = \mathrm{G}\mathrm{s}_{k-1}^{i_a}$, where $\mathrm{G} \in \mathbb{R}^{n_s\times n_s} = \mathrm{I}_2 \otimes \boldsymbol{\mathcal{G}}$, $\boldsymbol{\mathcal{G}} = \begin{bmatrix} 1 & T_{cpi} \\ 0 & 1 \end{bmatrix}$ and $T_{cpi}$ is the filter update time/radar CPI. Also, as $\mathbf{\Gamma}_a \mathrm{u}_k$ is modeling the acceleration term, the

$$\mathbf{\Gamma}_a = \begin{bmatrix} 0.5T_{cpi}^2 & 0 \\ T_{cpi} & 0 \\ 0 & 0.5T_{cpi}^2 \\ 0 & T_{cpi} \end{bmatrix}.$$

The DWNA motion model enables the adaptation of the target's movement based on the acceleration variances $(\sigma_{a_x}, \sigma_{a_y})$, as described in Eq. 15. For example, low acceleration variances represent the target's motion as a constant velocity, while higher variances capture the target's unpredictable motion, reflecting varying speeds. Therefore, the DWNA model allows us to have flexibility by adjusting the acceleration variances to suitable levels, and thus the model can accurately depict the movement of targets with complex and random paths.

The measurement model using the Kalman filter for the $i_a^{th}$ track ($\mathrm{o}_k^{i_a} \in \mathbb{R}^{2\times 1}$) is given by[2]

$$\mathrm{o}_k^{i_a} = \mathrm{h}(\mathrm{s}_k^{i_a}) + \mathrm{w}_k, \forall i_a \in [1, 2, \cdots, I] \tag{16}$$

where, $\mathrm{h}(\mathrm{s}_k^{i_a}) = \mathrm{H}\mathrm{s}_k^{i_a}$ and $\mathrm{H} = \begin{bmatrix} 1 & 0 & 0 & 0 \\ 0 & 0 & 1 & 0 \end{bmatrix}$ is the measurement matrix, $\mathrm{w}_k \in \mathbb{R}^{2\times 1}$ accounts for the error in modeling $\mathrm{o}_k^{i_a}$. Similar to $\mathrm{u}_k$, the $\mathrm{w}_k$ is also the Gaussian distributed sample with zero mean and a known covariance $\mathrm{R}_o = \mathbb{E}[\mathrm{w}_k \mathrm{w}_k{}^T]$, i.e. $\mathrm{w}_k \sim \mathcal{N}(0, \mathrm{R}_o)$.

Using the state and measurement model described in Eqs. 15 and 16, respectively, and for known G and H, the Kalman filter performs the prediction and update for $\forall i_a \in [1, 2, \cdots, I]$ as

$$\text{States Prediction} \quad \hat{\mathrm{s}}_k^{i_a} = \mathrm{G}\hat{\mathrm{s}}_{k-1}^{i_a}, \quad \mathrm{P}_k^{i_a} = \mathrm{G}\mathrm{P}_{k-1}^{i_a}\mathrm{G}^T + \mathrm{U}_\mathrm{s}, \tag{17}$$

where $\mathrm{U}_\mathrm{s} = \mathbf{\Gamma}_a \mathrm{U} \mathbf{\Gamma}_a^T$.

$$\text{States Update} \quad \mathrm{o}_k^{i_a} = \mathrm{H}\hat{\mathrm{s}}_k^{i_a}, \quad \mathrm{K}^{i_a} = \mathrm{P}_k^{i_a}\mathrm{H}^T(\mathrm{H}\mathrm{P}_k^{i_a}\mathrm{H}^T + \mathrm{R}_o)^{-1}, \quad \hat{\mathrm{s}}_k^{i_a} = \hat{\mathrm{s}}_k^{i_a} + \mathrm{K}^{i_a}(\mathrm{O}_k^{i_a} - \mathrm{o}_k^{i_a}), \quad \mathrm{P}_k^{i_a} = \mathrm{P}_k^{i_a} - \mathrm{K}^{i_a}\mathrm{H}\mathrm{P}_k^{i_a}.$$

[2] In the current work, a point target is considered, meaning that the detector reports only a single detection per target. However, if extended targets are present, they can be approximated as point targets by grouping the extended detections.

(18)

Using $\hat{\mathrm{s}}_k^{i_a}$, $\mathrm{O}_k^{p^{i_a}}$ in Eq. 14 is computed as $\mathrm{O}_k^{p^{i_a}} = \mathrm{H}\hat{\mathrm{s}}_k^{i_a}$. The updated values of $\mathrm{O}_k^{p^{i_a}}$ are then used in the next scan, that is, in the instance $k+1^{st}$ for data association. In the case of miss detections at the $k+1^{st}$ instance, where measurements may not be available in $\mathrm{O}_k$ for some existing tracks, their states are updated using the predicted measurements from the $k^{th}$ instance as

$$\hat{\mathrm{s}}_{k+1}^{i_a} = \hat{\mathrm{s}}_{k+1}^{i_a} + \mathrm{K}^{i_a}(\mathrm{O}_{k+1}^{i_a} - \mathrm{O}_k^{p^{i_a}}). \tag{19}$$

**Tracks Deletion** If the tracker continuously misses measurements for any existing tracks, then two scenarios are possible: (a) the target has permanently left the scene, or (b) due to sensor anomalies, such as limited FOV or restricted range, the measurements are missed. In scenario (b), where measurements have been missed for a few scans, the tracker should continue updating the states of the tracks using Eq. 19. In scenario (a), the tracks should be deleted. The tracker handles these scenarios automatically by introducing a delete counter for each track, denoted as ($\mathrm{d}_c \in \mathbb{N}^{1\times I}$). Each time a missed detection occurs, the delete counter for the corresponding track is incremented and compared against a predefined threshold. If the counter exceeds the threshold, the track is deleted. Otherwise, the state of the track is maintained using Eq. 19. Track deletion is implemented by removing the corresponding entry from $\mathrm{O}_k^p$, ensuring that future scans will not associate any measurements from $\mathrm{O}_k$ with deleted tracks.

## 3.2 Confirmation and Initialization of Tracks

**Initialization of Tracks** The unassociated $(M-I)$ measurements, which lack corresponding entries in $\mathrm{O}_k^p$, are analyzed in the next step to create new tracks. The creation of these new tracks leverages the idea that detections from the same target can be grouped together using distance metrics, facilitating their clustering. The number of clusters identified will directly correspond to the number of new tracks formed. In order to cluster the unassociated detections, the DBSCAN algorithm is utilized in this work.

Let $\mathrm{O}_k^{i_a}$ represent the set of associated measurements; then the unassociated measurements can be indicated by $(\mathrm{O}_k^{u_a} = \mathrm{O}_k \setminus \mathrm{O}_k^{i_a})$ and will accumulate for every consecutive scan, resulting in a new set $\mathrm{O}_k^{cl} = [\mathrm{O}_{k-1}^{cl}, \mathrm{O}_k^{u_a}]$ of unassociated measurements. The set $\mathrm{O}_k^{cl}$ will be processed further via the DBSCAN algorithm to get the clusters and their corresponding labels. For example, in the $k^{th}$ scan, suppose that the DBSCAN algorithm detects $\mathcal{C}$ clusters; the identified $\mathcal{C}$ clusters would be potential new tracks. Thus, for each group index of $i_c \in [1, 2, \ldots, \mathcal{C}]$, the corresponding measurements $\mathrm{O}_k^{cl^{i_c}}$ are treated as predicted measurements for newly formed $\mathcal{C}$ tracks. Unclustered measurements that are not members of any one of the $\mathcal{C}$ clusters are finally declared a cluttered effect and are nominated as false alarms. As $\mathrm{O}k^p$ is the set of measurements associated with the existing tracks, the new associated measurements $\mathrm{O}k^{cl^{i_c}}$ are added to $\mathrm{O}_k^p$ as follows: $\mathrm{O}_k^p = [\mathrm{O}_k^p, \mathrm{O}_k^{cl^{i_c}}]$. Along with updating $\mathrm{O}_k^p$, the state estimates $\hat{\mathrm{s}}_k^{i_c}$ and the error covariance matrices $\mathrm{P}_k^{i_c}$ for newly formed $\mathcal{C}$ tracks are initialized as $0_{n_s\times 1}$ and $\mathrm{I}_{n_s\times n_s}$, respectively.

**Confirmation of Tracks** The newly generated tracks, represented by the updated estimates $\hat{\mathrm{s}}_k^{ic}$ for each $i_c \in [1, 2, \ldots, \mathcal{C}]$, are initially labeled tentative. These tracks become confirmed only after undergoing a series of updates on successive scans. This process is managed by a confirmation counter, denoted by $\mathrm{c}_c \in \mathbb{N}^{1\times\mathcal{C}}$, whose element is associated with each tentative track. Each time a track is updated, the corresponding counter in $\mathrm{c}_c$ increases by 1. At each scan, the counter is compared with a pre-defined threshold. If the counter exceeds the threshold for a particular tentative track, that track is confirmed. Otherwise, the tentative track remains in the same state and will eventually be deleted following the track deletion procedure described in Subsection 3.1.

Algorithm 1 outlines the steps for implementing the proposed tracking algorithm, while Table 1 provides an explanation of the symbols used in Algorithm 1.

**Table 1** Explanation of characters used in Algorithm 1.

| Character | Explanation |
|---|---|
| $T_f$ | Maximum frame interval |
| $r_0$ | Noise variance along coordinate axis |
| $\delta_2^d$ | Threshold to delete the track |
| $\delta_2^c$ | Threshold to confirm the track |
| $\mathbf{d_c}$ | Counter to delete track |
| $\mathbf{c_c}$ | Counter to confirm track |
| $\emptyset$ | Null set for deletion of the entry |
| $\mathrm{T}_t, \mathrm{C}_t$ | Array to store the track information for tentative and confirmed track, respectively |

**Algorithm 1:** Pseudo code for the proposed tracking algorithm.

**Data:** $r$, $\mathbf{O}_k$, $T_f$, $I$, $T_{cpi}$, $n_s$, $\mathbf{U}_s = \mathbf{\Gamma}_a \mathbf{U} \mathbf{\Gamma}_a^T$, $\sigma_{a_x}, \sigma_{a_y}$, $\mathbf{R}_o = r_o \mathbf{I}_2$, $r_o$, $P_{fa}$, $P_d$, $\delta_1^c$, $\delta_2^d$

initialization: $\mathbf{d}_c$, $\mathbf{c}_c$, $\mathbf{O}_0^p$, $\mathbf{O}_{k-1}^{cl}$;
***Associating the Measurement:***
**while** $k <= T_f$ **do**
  **for** $i \leftarrow 1$ **to** $len(\mathbf{O}_{k-1}^p)$ **do**
    **for** $j \leftarrow 1$ **to** $len(\mathbf{O}_k)$ **do**
      $\mathcal{M}_{ij} = \exp\left( -(\mathbf{O}_{k-1}^{p^i} - \mathbf{O}_k^j) \sum_{k-1}^{i} (\mathbf{O}_{k-1}^{p^i} - \mathbf{O}_k^j)^H \right)$;
    **end**
    $\mathbf{d}_i = [\mathcal{M}_{i1}, \mathcal{M}_{i2}, \ldots, \mathcal{M}_{ij}, \ldots, \mathcal{M}_{iM}]$;
    $[val, indx] = \arg\min_j \mathbf{d}_i$;
    *Check if* $val < r$;
    **if** $val <= r$ **then**
      $j_i^a = indx$;
    **else**
      $j_i^a = 0$;
    **end**
    *Collect the corresponding associated measurement indexes in* $\mathbf{i}_a$;
    $\mathbf{i}_a = [j_1^a, j_2^a, \ldots, j_{i-1}^a, j_i^a]$;
  **end**
  ***Tracks updation using Kalman Filter***;
  **for** $i_a \leftarrow 1$ **to** $len(\mathbf{i}_a)$ **do**
    **if** $j_i^a \neq 0$ **then**
      *1)* Use (17) *to Perform Prediction*;
      *2)* Use (18) *to Perform Update*;
      *Tracks confirmation* ;
      **if** $\mathbf{c}_c^{i_a} \leq \delta_1^c$ **then**
        *Store the track information as tentative track*;
        $\mathbf{T}_t^{i_a} = \hat{\mathbf{s}}_k^{i_a}$;
        *As the* $i_a^{th}$ *track is updated the confirm counter will increment*
        $\mathbf{c}_c^{i_a} = \mathbf{c}_c^{i_a} + 1$;
      **else**
        *Store the track information as confirmed track*;
        $\mathbf{C}_t^{i_a} = \hat{\mathbf{s}}_k^{i_a}$;
      **end**
    **else**
      *If miss detections happens, the prediction and update steps remain identical to those in lines* 22 *and* 23. *However, due to the absence of measurements,* $\mathbf{O}_k^p$ *is used instead of* $\mathbf{O}_k$.;
      **if** $\mathbf{c}_c^{i_a} \leq \delta_1^c$ **then**
        $\mathbf{T}_t^{i_a} = \hat{\mathbf{s}}_k^{i_a}$;
        $\mathbf{c}_c^{i_a} = \mathbf{c}_c^{i_a} + 1$;
      **else**
        $\mathbf{C}_t^{i_a} = \hat{\mathbf{s}}_k^{i_a}$;
      **end**
      *As the measurement for* $i_a^{th}$ *track is missed the delete counter will increment*;
      $\mathbf{d}_c^{i_a} = \mathbf{d}_c^{i_a} + 1$;
    **end**
  **end**
  ***New tracks generation***;
  $\mathbf{O}_k^{ua} = \mathbf{O}_k \setminus \mathbf{O}_k^{\mathbf{i}_a}$;
  **if** $\mathbf{O}_k^{ua} \neq \emptyset$ **then** 12
    $\mathbf{O}_k^{cl} = [\mathbf{O}_{k-1}^{cl}, \mathbf{O}_k^{ua}]$;
    $[\mathcal{C}] = DBSCAN(\mathbf{O}_k^{cl})$;
    **for** $i_c \leftarrow 1$ **to** $len(\mathcal{C})$ **do**
      $\mathbf{O}_k^p = [\mathbf{O}_k^p, \mathbf{O}k^{cl^{i_c}}]$, $\hat{\mathbf{s}}_k^{i_c} = \mathbf{0}_{n_s \times 1}$, $\mathbf{P}_k^{i_c} = \mathbf{I}_{n_s \times n_s}$, $\mathbf{d}_c^{i_c} = 0$;
    **end**
  **else**
    *Terminate the if command*;
  **end**
  ***Tracks deletion***;
  **for** $d \leftarrow 1$ **to** $len(\mathbf{d}_c)$ **do**
    **if** $\mathbf{d}_c^d \geq \delta_2^d$ **then**
      $\mathbf{O}_k^{pd} = \emptyset$, $\hat{\mathbf{s}}_k^d = \emptyset$, $\mathbf{P}_k^d = \emptyset$, $\mathbf{dc}^d = 0$ ;
    **else**
      *Terminate the if command*;
    **end**
  **end**
**end**

### 3.3 MTT Scheme Computational Complexity

As shown in Figure 2, radar detection goes through several discrete connected steps before it is converted to a track. Therefore, the combined computational complexity of the tracker is the sum of the individual computational complexity of each step. The computational complexity is calculated for each radar frame/scan individually. In the following, the computational complexity of each step is mentioned sequentially.

1. The data association step implemented by the nearest neighbor algorithm will have a computing complexity of the order $\mathcal{O}(4IM)$.
2. Next, to check whether the unassociated measurements form a track, the DBSCAN algorithm is performed. Hence, the computational complexity of this stage is of the order $\mathcal{O}\big(\{M-I\}^2\big)$.
3. The associated $I$ measurements will be forward to the Kalman filter for the estimation of states. Therefore, this step includes the computational complexity of the order $\mathcal{O}(8I)$.

From the steps mentioned above, it is evident that the generation of new tracks via DBSCAN contributes significantly to the overall computational cost of tracking, and the combined computational complexity of the tracker is on the order of $\mathcal{O}(4IM + \{M-I\}^2 + 8I)$.

## 4 Simulation And Results

The simulations are organized into two main categories: Subsection 4.1 revisits the effectiveness of the detection method proposed in [14], while Subsection 4.2 assesses the performance of the proposed tracking system, which is based on the detector performance described in Subsection 4.1. Both scenarios are evaluated using the indoor surveillance scene shown in Figure 1. The performance of the detector and tracker is quantified using the post-processing signal-to-noise plus interference ratio ($\mathrm{SINR}_{\mathrm{Post}}$), which is defined as follows.

$$\mathrm{SINR}_{\mathrm{Post}} = \frac{1}{\sigma^2}\boldsymbol{\alpha}^H \mathrm{S}^H \mathrm{P}_{\mathrm{E}}^{\perp} \mathrm{S}\boldsymbol{\alpha} \tag{20}$$

### 4.1 Review of Target Detection Performance

This subsection re-assesses the performance of the detector proposed in [14]. Table 2 shows the parameter values of the sensors considered for the simulations in this work. In the sequel, the detection performance is analyzed which illustrates the advantages of using the network of MIMO radar sensors for indoor scene surveillance applications.

**Table 2** TI IWR6843ISK mmWave sensor Parameters

| Parameter | Value | Parameter | Value |
|---|---|---|---|
| $P_t$ | 12 dBm | $G_t$ | 0 dBi |
| $G_r$ | 34 dBi | $\lambda$ | 5 mm |
| $\sigma_l$ | 0.1 $m^2$ | $k_B$ | $1.38 \times 10^{-23}$ |
| $T_0$ | 290° $K$ | $B$ | 10 MHz |
| $F_n$ | 12 dB | $L_{sl}$ | 3 dB |
| $SNR_{min}$ | 2 dB | | |

In Figure 3, the detection performance is illustrated in terms of receiver operating characteristics (ROC) for different numbers of mmWave MIMO radars. In Figure 3a, scenarios with targets having identical RCS are considered in various sensor configurations. With an increasing number of sensors, the post-processing SINR improves, leading to better performance.

In contrast, Figure 3b maintains a constant post-processing SINR across all configurations, regardless of sensor count. To achieve this, the target's RCS is adjusted to ensure that both distributed and co-located setups receive equal SINR. Under these conditions, while both systems experience similar SINR from the target, the co-located system benefits from coherent integration, resulting in superior performance. Furthermore, Figure 3c shows that when the target amplitude fluctuates, the increase in the number of sensors improves the detection performance due to the benefits of RCS diversity, even with the same post-processing SINR.

### 4.2 Target Tracking Performance

In this subsection, we assess the performance of the proposed MTT technique for the distributed MIMO radar network[3]. The evaluation involves the maneuvering of three targets in an indoor environment, with the ground truth (GT) trajectories depicted in Figure 4. The tracker's measurements are derived from the detector's output, which includes information related to the $P_{fa}$ and $P_d$, as described by the GLRT-based detector in Eq. 12. The measurements consist of both target detections and spurious detections resulting from false alarms, as shown in Figure 4 for $P_{fa} = 10^{-5}$ and $P_d = 0.9$. Targets are assumed to be present throughout the entire observation period, although the availability or unavailability of target detections is determined by the value

[3] It is important to note that the developed tracker is innovative, and there is a lack of existing literature addressing trackers for distributed mmWave MIMO radar sensors. As a result, the performance of the proposed tracker is studied for the number of sensors ($L$).

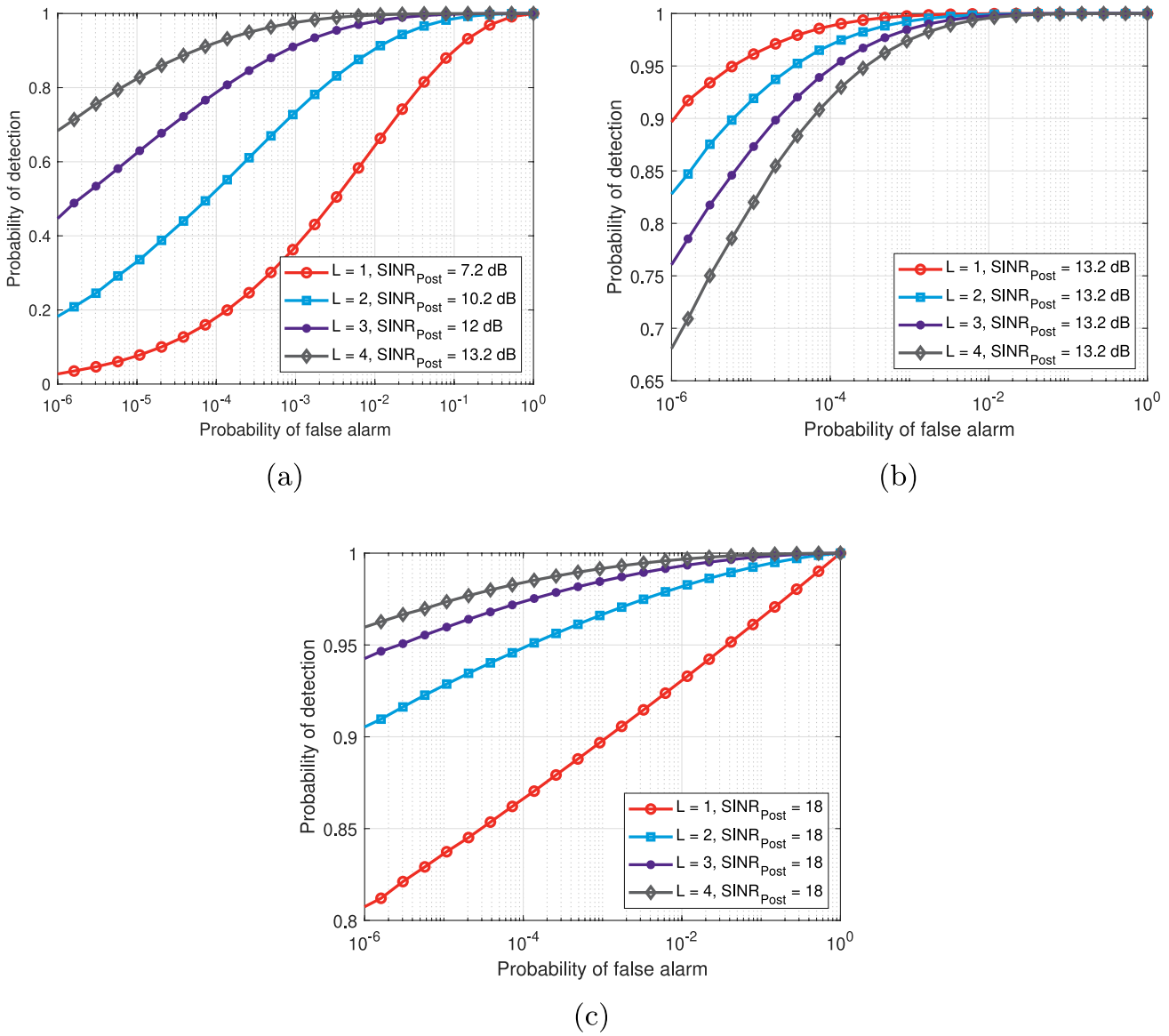


**Fig. 3** Detector performance with $L = 1, 2, 3, 4$ distributed sensors: a) targets with constant RCS (Swerling 0), b) the same $\mathrm{SINR}_{\mathrm{Post}}$ and constant RCS, and c) the same $\mathrm{SINR}_{\mathrm{Post}}$ with fluctuating RCS (Swerling 1).

of $P_d$. Tracker performance is evaluated on the basis of two key metrics: the number of tracks successfully maintained during the observation interval and the root mean square error (RMSE) in the estimation of the targets' positions. The RMSE is defined below.

$$RMSE = \sqrt{\frac{1}{KN}\sum_{k=1}^{K}\sum_{n=1}^{N}(\hat{x}_k^n - x_k^n)^2 + (\hat{y}_k^n - y_k^n)^2},$$

where $x_k^n$ and $y_k^n$ are the $n^{th}$ target true location at $k^{th}$ frame along $x$ and $y$ axes, respectively.

Scenario I: this corresponds to Figure 3a, in which targets with the same RCS (Swerling 0) for different sensor numbers are considered. As the RCS of the targets for the radar sensors is the same, the post-processing SINR improves with the increase in sensor number, and Scenario II: this corresponds to Figure 3c, i.e. fluctuating target amplitude, due to RCS diversity gain (Swerling I); however, unlike Scenario I, Scenario II has the same post-processing SINR. The performance of the tracker for Scenarios I and II is observed for different sensor numbers, that is, for $L = 1, 2, \cdots, 4$. In addition, for every $L$, the performance of the tracker is evaluated for different values of $P_{fa}$ and $P_d$ obtained from the detector Eq. 12.

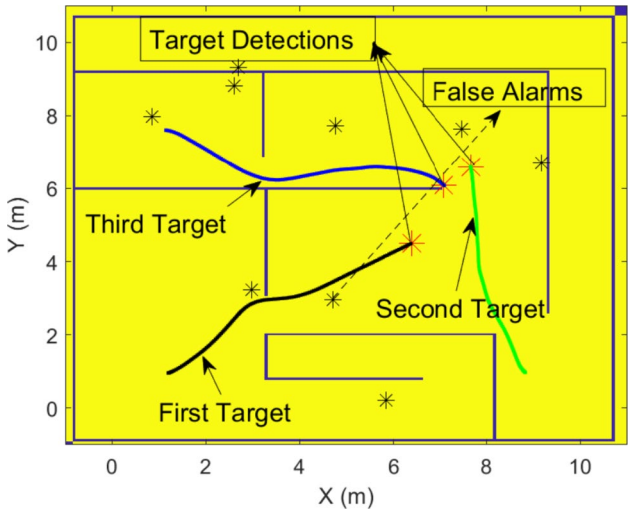


**Fig. 4** Targets' Ground truth in black, green, and blue for first target, second target, and third target, respectively. Target detections (red stars) and false alarms (black stars) for $P_d = 0.9$, and $P_{fa} = 10^{-5}$, respectively.

#### 4.2.1 Scenario I: Tracker Performance for the Swerling 0 Target Model

The number of tracks maintained by the tracker for $P_{fa} = 10^{-6}, 10^{-5}$ and $10^{-4}$ for the entire observation period is shown in Figure 5. As shown in Figure 5, for a low value of $P_{fa} = 10^{-6}, 10^{-5}$ and for $L = 4$, the tracker maintains the tracks for the true numbers of targets in the scene, which are three in this case. However, as $L$ decreases and hence $P_d$, the tracker starts to lose tracks and does not maintain the tracks for the true number of targets. In addition, the number of tracks maintained by the tracker is not consistent. For example, the number of tracks maintained by the tracker decreases as $P_d$ decreases. In Table 3, the tracker's RMSE performance for $P_{fa}$ and $L$ are summarized. As mentioned in Table 3, particularly for $P_{fa} = 10^{-6}$ and $P_{fa} = 10^{-5}$, the RMSE increases as $L$ decreases. Also, because of the better $P_d$, the tracker's RMSE performance for $P_{fa} = 10^{-5}$ is better than the RMSE performance for $P_{fa} = 10^{-6}$.

For high $P_{fa}$ ($P_{fa} = 10^{-4}$), the tracker performance is shown in Figure 5c, and the relevant RMSEs for different $L$ are shown in Table 3. Although by virtue of high $P_d$ the RMSE is improved, but at the cost of generating false tracks, as shown in Figure 5c. With the aforementioned study and referring to Figure 3a and Table 3, it can be concluded that the detector's ROC and tracker's RMSE performance improve with increasing $L$. Moreover, as a matter of fact, the improvement in the RMSE performance of the tracker with $L$ is independent of $P_{fa}$. However, as Figure 5c suggests, for optimal tracking results, the designed detector and tracker should be operated around $P_{fa} = 10^{-5}$ to avoid losing the tracks and creating false tracks.

#### 4.2.2 Scenario II: Tracker Performance for the Swerling 1 Targets Model

The number of tracks maintained by the tracker for $P_{fa} = 10^{-6}, 10^{-5}$ and $10^{-4}$ relevant to Scenario II, is shown in Figure 6. The respective RMSE performances are shown in the Table 4. As shown in Figure 6 and Table 4, unlike Scenario I, for low $P_{fa} = 10^{-6}, 10^{-5}$ the tracker maintained the true number of targets irrespective of $P_d$ and $L$. This behavior is justified in Figure 3c, in which the slight change in $P_d$ is illustrated by the increase in $L$. Consequently, the change in $L$ would not affect the tracker's performance. However, as Figure 6c suggests, for high $P_{fa} = 10^{-4}$, and regardless of $L$, the tracker generates false tracks which resulted in high RMSEs as shown in Table. 4. From this study, it can be concluded that in the case of the Swerling 1 target, the creation of false tracks could be avoided by setting the detector's $P_{fa}$ between $10^{-5}$ and $10^{-6}$.

The readers interested in the real-time implementation of the proposed MTT scheme are encouraged to refer to [24].

### 4.3 Comparison with the Classical Approach

The presented work utilizes a novel detector that, unlike conventional detection methods, utilizes a signal model that includes signal-dependent and signal-independent interferences. These interferences have varying coefficients based on the geometry and reflectivity of each interfering source. As a result, the detector (named subspace detector: for comparison) outperforms classical detectors (such as Kelly and adaptive matched filter (AMF) [25, 26]) when the clutter-to-noise ratio (CNR) in the subspace of interest exceeds the loss of the orthogonal subspace matrix. This is because the Kelly and AMF detectors are based on interference covariance matrix estimation, and when there is no perfect information about the interference statistics, the detector fails to yield the optimum results. However, unlike classical detectors, the detector considered in this work is based on knowledge about the subspace of the interface and suppresses the interface component of the received signal using the orthogonal projection matrix. In Figure 7, the performance of the detector and the tracker is depicted compared to the classical approach. In particular, as shown in Figure 7a, the subspace detector is exceeding the classical detectors, especially in the high clutter-to-noise ratio (CNR) regime. The corresponding improvement in tracking performance is shown in Figure 7b for the number of

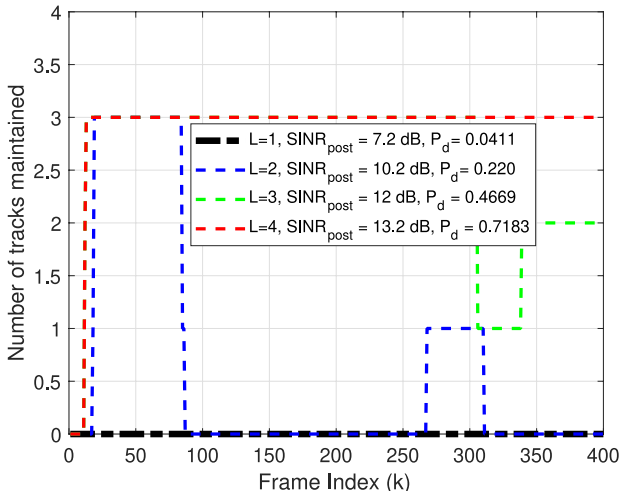


(a) $P_{fa} = 1.6 \times 10^{-6}$

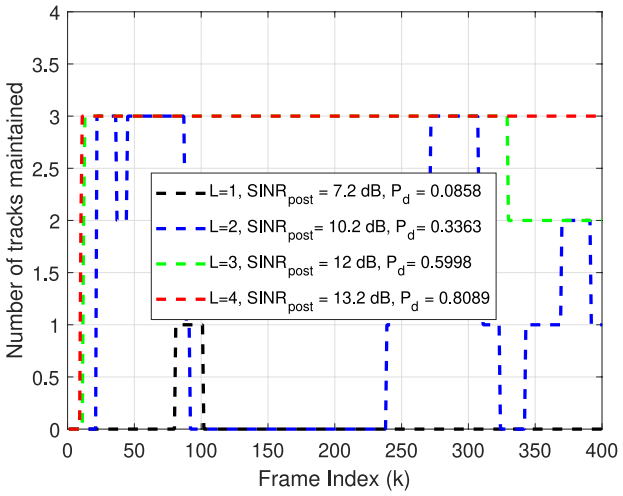


(b) $P_{fa} = 10^{-5}$

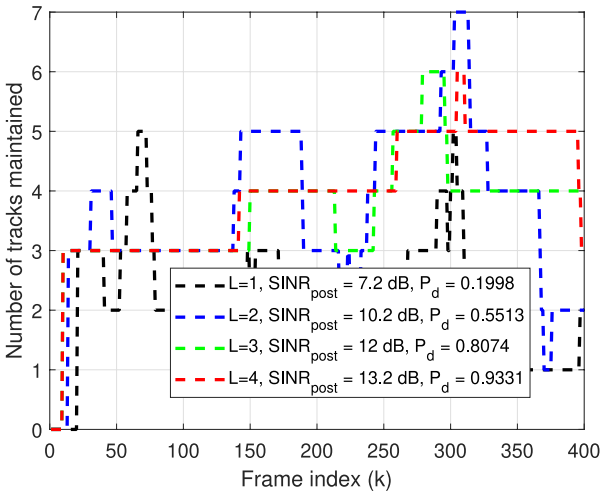


(c) $P_{fa} = 10^{-4}$

**Fig. 5** Number of tracks maintained by the proposed tracker for Swerling 0 targets and for (a) $P_{fa} = 1.6 \times 10^{-6}$, (b) $P_{fa} = 10^{-5}$, and (c) $P_{fa} = 10^{-4}$.

sensors $Q = 4$. From Figure 7a it is explicit that the subspace-based detector provides the detection with better $P_{\mathrm{D}}$ and $P_{\mathrm{FA}}$ and consequently the proposed tracker maintains the tracks for the true number of targets. In contrast, the performance obtained by the tracker utilizing the Kelly and AMF detections is erroneous and not capable of maintaining the tracks for true targets for all the radar scans.

## 5 Conclusion

An MTT scheme is proposed for the distributed monostatic MIMO radar network. The paper first reviews a GLRT-based detector for the distributed mmWave MIMO radar, which exploits a lower-dimensional clutter subspace. This is followed by an analytical evaluation of the detector performance, providing valuable insight into the functionality of the system. Subsequently, an MTT scheme is introduced to track multiple target movements using detector detections. The proposed tracker incorporates an effective track

**Table 3** Tracker's RMSE Performance for Swerling 0 (Scenario I) targets model.

| $L$ | $P_{fa} = 10^{-6}$ | $P_{fa} = 10^{-5}$ | $P_{fa} = 10^{-4}$ |
|---|---|---|---|
| 1 | 8.0545 m | 7.3787 m | 2.7204 m |
| 2 | 6.9322 m | 5.7224 m | 0.2602 m |
| 3 | 2.5084 m | 0.1691 m | 0.1773 m |
| 4 | 0.1671 m | 0.1605 m | 0.1707 m |

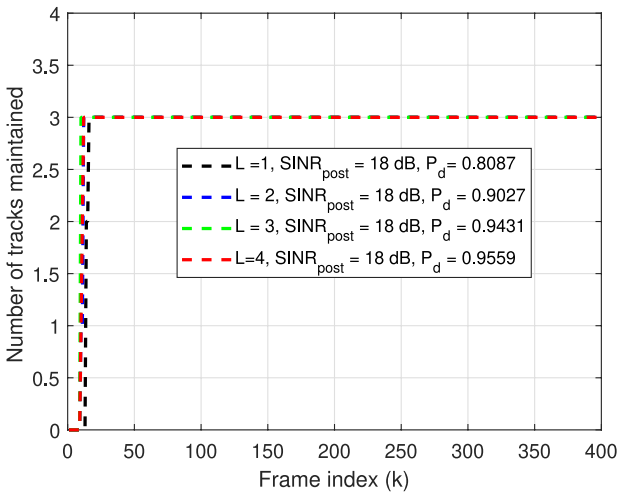


(a) $P_{fa} = 10^{-6}$

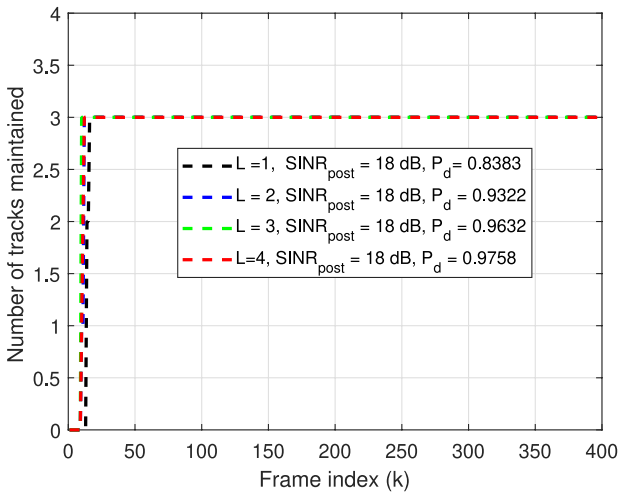


(b) $P_{fa} = 10^{-5}$

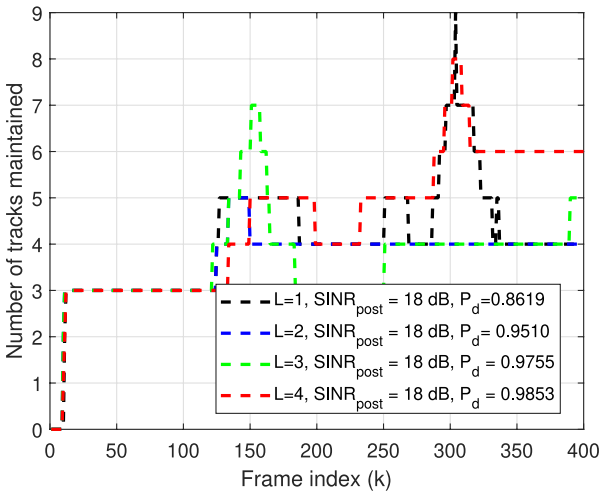


(c) $P_{fa} = 10^{-4}$

**Fig. 6** Number of tracks maintained by the proposed tracker for Swerling 1 targets and for (a) $P_{fa} = 1.6 \times 10^{-6}$, (b) $P_{fa} = 10^{-5}$, and (c) $P_{fa} = 10^{-4}$.

maintenance mechanism that efficiently handles false alarms and missed detections. The simulation results obtained conclude that the scenarios in which targets RCS are non-fluctuating, in terms of both detection and tracking performance, and even for an identical post-processing SINR, a single colocated MIMO radar outperforms distributed configurations. However, in more practical cases, where different post-processing SINR and constant RCS targets are considered, the distributed radar configuration demonstrates superior performance. Additionally, when RCS fluctuates, the distributed radar configuration benefits from its ability to observe targets from various aspect angles and exploit RCS diversity, outperforming a single co-located MIMO radar. Moreover, in the case of targets' RCS fluctuations, improved performance is observed even at equivalent

**Table 4** Tracker's RMSE performance for Swerling 1 (Scenario II) targets model.

| $L$ | $P_{fa} = 10^{-6}$ | $P_{fa} = 10^{-5}$ | $P_{fa} = 10^{-4}$ |
|---|---|---|---|
| 1 | 0.1635 m | 0.1628 m | 0.1969 m |
| 2 | 0.1631 m | 0.1615 m | 0.1637 m |
| 3 | 0.1627 m | 0.1606 m | 0.1653 m |
| 4 | 0.1619 m | 0.1607 m | 0.2035 m |

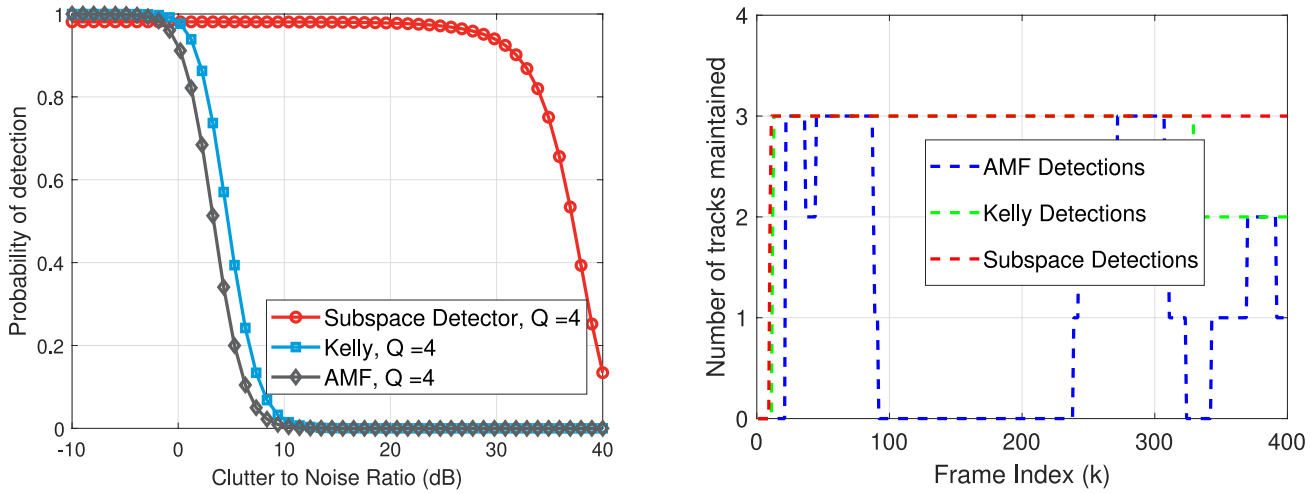


(a) Detector Performance (b) Corresponding Tracker Performance

**Fig. 7** The comparative performance of (a) Detector and (b) Tracker with the classical Kelly and AMF approach for $Q = 4$.

post-processing SINR levels. The proposed approach has demonstrated a significant advantage over the classical approach. Finally, optimal tracking performance for both fluctuating and non-fluctuating RCS cases is achieved when $P_{fa}$ is approximately $10^{-5}$.

**Funding** Financial support has not been provided for the work presented.

**Data Availability** Real-time data are not used for the presented work. The experimental analysis is performed on simulated data.

## Declarations

**Conflicts of Interest** We declare no conflict of interest with respect to the presented work.

## References

1. Ghotbi, S., Ahmadi, M., & Sebt, M.A. (2014). Moving target detection in airborne MIMO radar for fluctuating target RCS model. In: *2014 22nd European Signal Processing Conference (EUSIPCO)*, pp. 1701–1705.
2. Liu, J., & Li, J. (2019). Robust detection in MIMO radar with steering vector mismatches. *IEEE Transactions on Signal Processing, 67*(20), 5270–5280. https://doi.org/10.1109/TSP.2019.2939078
3. Li, H., Wang, F., Zeng, C., & Govoni, M. A. (2021). Signal detection in distributed MIMO radar with non-orthogonal waveforms and sync errors. *IEEE Transactions on Signal Processing, 69*, 3671–3684. https://doi.org/10.1109/tsp.2021.3087897
4. Gao, X., Xing, G., Roy, S., & Liu, H. (2019). Experiments with mmwave automotive radar test-bed. In: *2019 53rd Asilomar Conference on Signals, Systems, and Computers*, pp. 1–6. https://doi.org/10.1109/IEEECONF44664.2019.9048939
5. Richards, M. A. (2005). Fundamentals of Radar Signal Processing. Tata McGraw-Hill Education.
6. He, Q., Lehmann, N. H., Blum, R. S., & Haimovich, A. M. (2010). Mimo radar moving target detection in homogeneous clutter. *IEEE Transactions on Aerospace and Electronic Systems, 46*(3), 1290–1301. https://doi.org/10.1109/TAES.2010.5545189
7. Li, H., Wang, F., Zeng, C., & Govoni, M. A. (2021). Signal detection in distributed MIMO radar with non-orthogonal waveforms and sync errors. *IEEE Transactions on Signal Processing, 69*, 3671–3684. https://doi.org/10.1109/TSP.2021.3087897
8. Wang, P., Li, H., & Himed, B. (2011). Moving target detection using distributed MIMO radar in clutter with nonhomogeneous power. *IEEE Transactions on Signal Processing, 59*(10), 4809–4820. https://doi.org/10.1109/TSP.2011.2160861
9. Ghotbi, S., Ahmadi, M., & Mohamedpour, K. (2015). Moving target detection under spatially non-homogeneous clutter for airborne phased-MIMO radar. In: *2015 IEEE Radar Conference*, pp. 82–86. https://doi.org/10.1109/RadarConf.2015.7411859
10. Safa, A., Verbelen, T., Keuninckx, L., Ocket, I., Hartmann, M., Bourdoux, A., Catthoor, F., & Gielen, G. G. E. (2021). A low-complexity radar detector outperforming os-cfar for indoor drone obstacle avoidance. *IEEE Journal of Selected Topics in Applied Earth Observations and Remote Sensing, 14*, 9162–9175. https://doi.org/10.1109/JSTARS.2021.3107686
11. Wang, S., & Herschel, R. (2022). Fast 3D-CFAR for drone detection with MIMO radars. In: *2021 18th European Radar Conference (EuRAD)*, pp. 209–212. https://doi.org/10.23919/EuRAD50154.2022.9784486
12. Xu, C., Wang, F., Zhang, Y., Xu, L., Ai, M., & Yan, G. (2021). Two-level CFAR algorithm for target detection in mmWave radar. In: *2021 International Conference on Computer Engineering and Application (ICCEA)*, pp. 240–243. https://doi.org/10.1109/ICCEA53728.2021.00055
13. Liu, J., Jin, D., Liu, W., Orlando, D., & Farina, A. (2022). Polarimetric GLRT for adaptive detection in general array configuration. *IEEE Transactions on Signal Processing, 70*, 4201–4211. https://doi.org/10.1109/TSP.2022.3198862
14. Ahmadi, M., Alaee-Kerahroodi, M., MR, B. S., & Ottersten, B. (2023). Subspace-based detector for distributed mmwave mimo radar sensors. In: *ICASSP 2023 - 2023 IEEE International Conference on Acoustics, Speech and Signal Processing (ICASSP)*, pp. 1–5. https://doi.org/10.1109/ICASSP49357.2023.10095315
15. Palacios, J., Bielsa, G., Casari, P., & Widmer, J. (2019). Single- and multiple-access point indoor localization for millimeter-wave

networks. *IEEE Transactions on Wireless Communications, 18*(3), 1927–1942.
16. Bar-Shalom, Y., Fortmann, T. E., & Cable, P. G. (1990). Tracking and data association. Acoustical Society of America.
17. Leung, H., Hu, Z., & Blanchette, M. (1999). Evaluation of multiple radar target trackers in stressful environments. *IEEE Transactions on Aerospace and Electronic Systems, 35*(2), 663–674. https://doi.org/10.1109/7.766946
18. Marveldoss, W. D., Joshika, B., & Sebastian, B. (2024). Tracking and estimation approach for human-aware mobile robot navigation. *IEEE Sensors Letters, 8*(12), 1–4. https://doi.org/10.1109/LSENS.2024.3492373
19. Singh, U. K., Alaee-Kerahroodi, M., & Bhavani Shankar, M. R. (2022). Implementation and Validation of Multiple Target Tracking Technique for Indoor Applications. In: *2022 IEEE International Conference on Advanced Networks and Telecommunications Systems (ANTS)*, pp. 219–224. https://doi.org/10.1109/ANTS56424.2022.10227719
20. Blackman, S. S. (1986). Multiple-target tracking with radar applications. Dedham.
21. Singh, U. K., Alaee-Kerahroodi, M., Shankar, M. R. B., & Thipparaju, R. R. (2024). Mee-based adaptive state estimator for non-gaussian radar measurement. In: *2024 IEEE Radar Conference (RadarConf24)*, pp. 1–6. https://doi.org/10.1109/RadarConf2458775.2024.10548434
22. Singh, U. K., Alaee-Kerahroodi, M., & Bhavani Shankar, M. R. (2023). Rkhs based dynamic state estimator for non-gaussian radar measurements. In: *2023 IEEE Radar Conference (RadarConf23)*, pp. 1–6. https://doi.org/10.1109/RadarConf2351548.2023.10149463
23. Chen, Y., Zhou, L., Pei, S., Yu, Z., Chen, Y., Liu, X., Du, J., & Xiong, N. (2021). KNN-BLOCK DBSCAN: Fast clustering for large-scale data. *IEEE Transactions on Systems, Man, and Cybernetics: Systems, 51*(6), 3939–3953. https://doi.org/10.1109/TSMC.2019.2956527
24. Singh, U. K., & Thipparaju, R. R. (2025). Online targets tracking and people counting using multiple distributed mmwave radar sensors. *Progress in Electromagnetics Research C 155*
25. Liu, W., Xie, W., & Wang, Y. (2014). Parametric detector in the situation of mismatched signals. *IET Radar, Sonar & Navigation, 8*(1), 48–53.
26. Kelly, E. J. (2007). An adaptive detection algorithm. *IEEE transactions on aerospace and electronic systems, 2*, 115–127.